Lecture 3

the nucleon radius, a crisis and its resolution

The nucleon is one of the basic building blocks of matter around us and in the universe. As discussed in Lecture 2, understanding its properties is a key element of the human scientific enterprise. Much of the effort in this direction has not fully concluded. This lecture is about the size of the proton or, more precisely, about a precision determination of its charge density distribution.

Information about the charge density distribution and the connected quantity of the rms radius of this distribution, can be obtained by scattering charged leptons, electrons or muons, off a hydrogen target. Alternatively, one can make precision measurements of the atomic structure of H, and of μH, where the electron is replaced by a muon. The finite size of the protons leads to changes in both measurements.

We first introduce the electron scattering experiments and later report on the most recent atomic structure experiments.

Mott cross section

Differential cross-section for scattering of spin-½ electrons from a pointlike (spin 0) target is given by the "**Mott cross-section**", which is the Rutherford result multiplied by $\cos^2(\theta/2)$ and a "recoil factor" E'/E_o

$$\frac{d\sigma}{d\Omega}|_{Mott} = \frac{(\alpha)^2}{4E_o^2 \sin^4(\theta/2)}\left(\frac{E'}{E_o}\right)\cos^2(\theta/2)$$

$$= \frac{(\alpha)^2 \cos^2(\theta/2)}{4E_o^2 \sin^4(\theta/2)\left[1 + 2\frac{E_o}{M}\sin^2(\theta/2)\right]}$$

In terms of the **4-momentum transfer, Q^2**, the result for an **extended spin ½ target**, with both electric charge and magnetization distributions, is formulated in terms of **electric and magnetic form factors**:

$$G_E(Q^2) \text{ and } G_M(Q^2) \ldots$$

note: the $\cos^2(\theta/2)$ factor corresponds to the non spin-flip amplitude, for spin-flip we expect a factor proportional to $\sin^2(\theta/2)$

Summary of elastic e-p scattering

$Q^2 = -q^2$

$$-q^2 = 4EE'\sin^2\frac{\theta}{2}$$

General form of diff. cross section

$$\frac{d\sigma}{d\Omega} = \frac{\alpha^2}{4EE'\sin^4\frac{\theta}{2}} \cdot \frac{E'}{E}\{\ldots\}$$

Rutherford

non pointlike scattering partners w/ spin

recoil

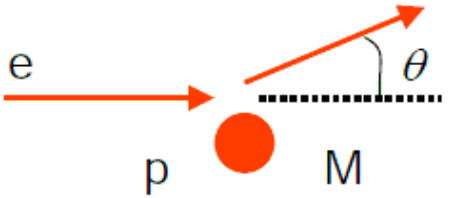

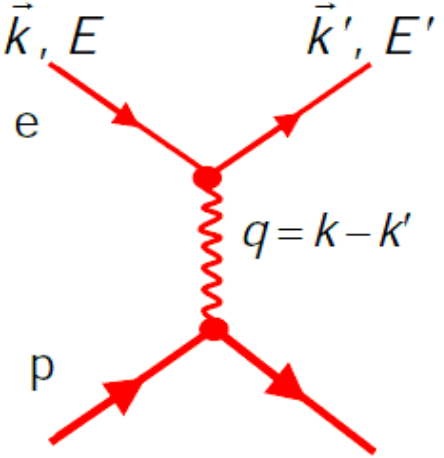

Pointlike target w/o spin Mott scattering

$$\{\ldots\}^{elastic}_{Mott} = \left(\cos^2\frac{\theta}{2}\right)$$

Pointlike target w/ spin

$$\{\ldots\}^{elastic}_{e\mu\to e\mu} = \left(\cos^2\frac{\theta}{2} - \frac{q^2}{2M^2}\sin^2\frac{\theta}{2}\right)$$

Extended proton w/ spin

$$\{\ldots\}^{elastic}_{ep\to ep} = \left(\frac{G_E^2 + \tau G_M^2}{1+\tau}\cos^2\frac{\theta}{2} - 2\tau G_M^2\sin^2\frac{\theta}{2}\right) \quad \text{mit } \tau = \frac{q^2}{4M^2}$$

Dirac scattering and the Rosenbluth separation formula

$$\frac{d\sigma}{d\,\Omega} = \left(\frac{d\sigma}{d\,\Omega}\right)_{Mott} \left\{ \left(\frac{G_E^2 + \tau \;\; G_M^2}{1 + \tau} \right) + 2\tau \;\; G_M^2 \; tan^2(\theta/2) \right\}, \; with \; \tau \equiv \frac{Q^2}{4\mathrm{M}^2}$$

Rosenbluth separation

$$\frac{d\sigma}{d\Omega} = \left(\frac{d\sigma}{d\Omega}\right)_{Mott} \left\{ \left(\frac{G_E^2 + \tau \; G_M^2}{1+\tau} \right) + 2\tau \; G_M^2 \, tan^2(\theta/2) \right\}, \; with \; \tau \equiv \frac{Q^2}{4M^2}$$

- both electric and magnetic form factors contribute to the scattering
- to disentangle the two contributions, one has to compare measurements at the **same Q^2** but **different scattering angles**

"Rosenbluth separation method":

$$\frac{\frac{d\sigma}{d\Omega}}{\left(\frac{d\sigma}{d\Omega}\right)_{Mott}} = \left\{ A(Q^2) + B(Q^2) \, tan^2 \frac{\theta}{2} \right\}$$

Example: e-p scattering

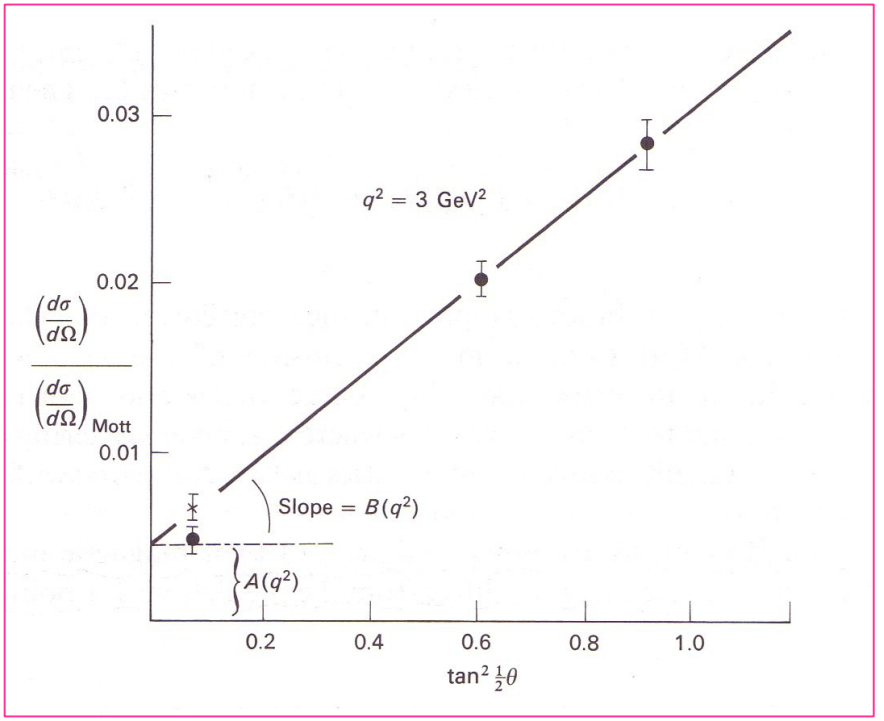

Form factors of the proton

electric:

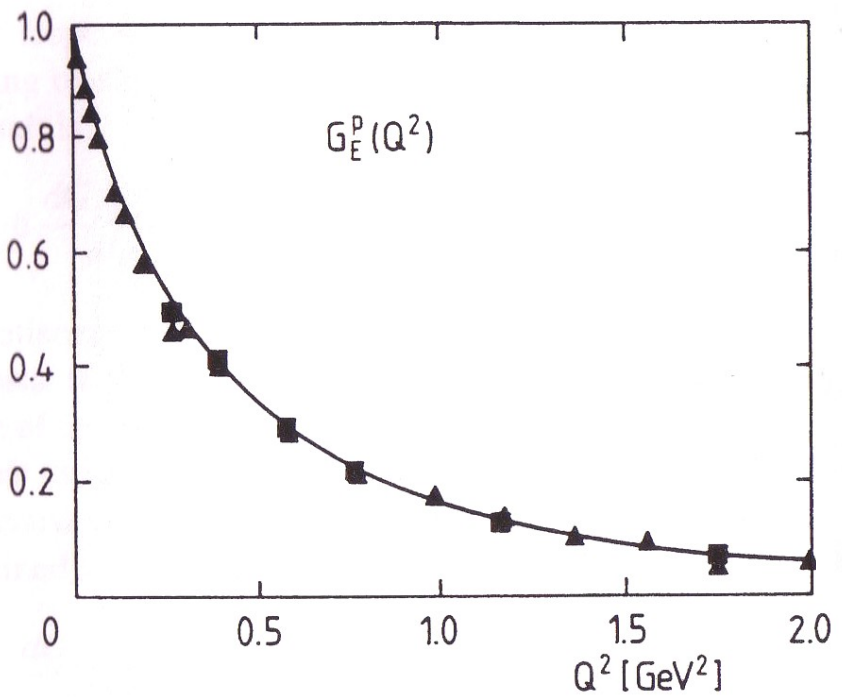

magnetic:

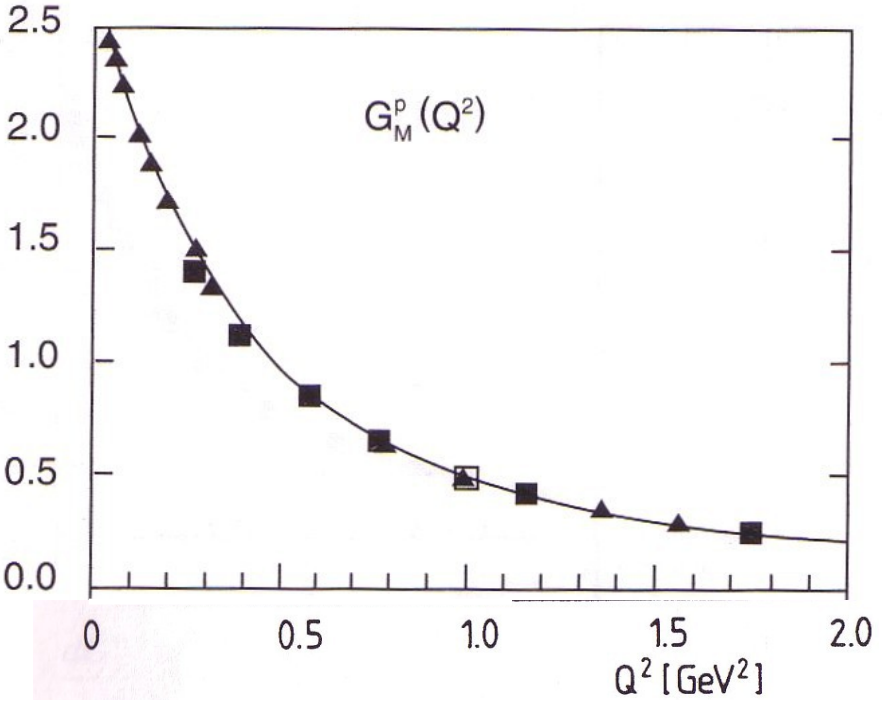

Same shape!!! scaling relation:

$$G_E^p(Q^2) = G_M^p(Q^2)/\mu_N = \frac{1}{(1+Q^2/0.71)^2}$$

The charge distribution of the static proton

- charge and magnetization distributions are very similar
- both form factors follow a "dipole" pattern, e.g.

$$G_E^p(Q^2) = \frac{1}{(1 + Q^2/0.71\ GeV^2)^2}$$

- measurements from Jefferson Lab (USA) show that the charge and magnetization distributions differ at higher Q for reasons that are now understood as due to 2-photon exchange processes
- inelastic scattering -> quark parton structure

Electric charge distribution:

$$\rho(r) = e\rho_o \exp(-M r)$$

$$M = 4.33\ fm^{-1}$$

$$\langle r^2 \rangle^{1/2} = \frac{\sqrt{12}}{M} = 0.80\ fm$$

sketch based on early results from the 1960ties. see references in the following.

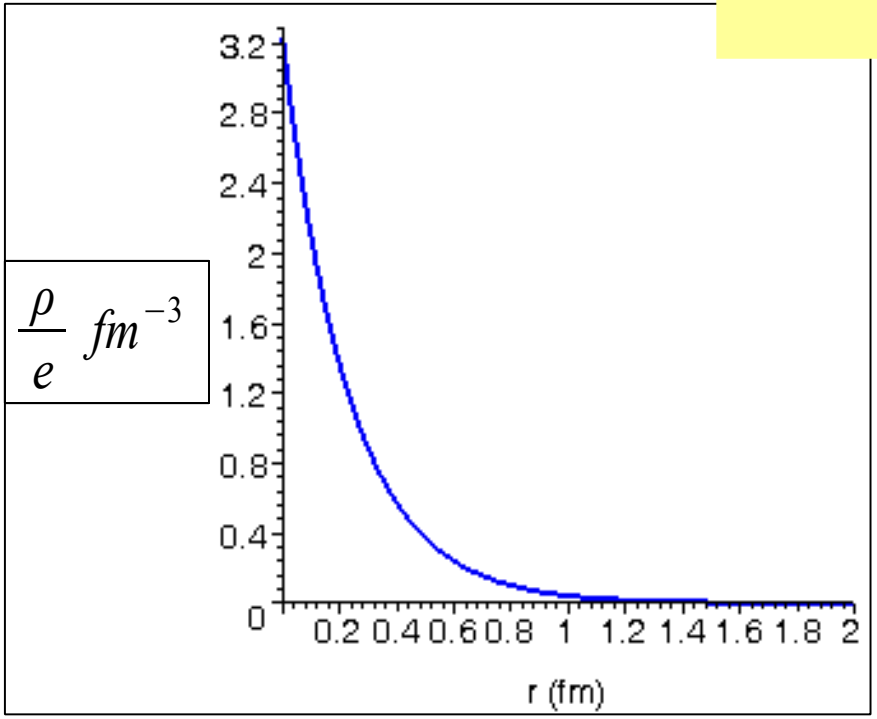

Note: the charge inside the proton is not distributed corresponding to a uniform distribution of a charged sphere, but looks nearly exponential.

A note on form factors and rms radii

We only deal with the low Q^2 region where $\tau \ll 1$

$$\Rightarrow \frac{d\sigma}{d\Omega} = \sigma_{Mott} \cdot G_E^2 \qquad \langle r^2 \rangle = \int_0^\infty \rho(r)\, r^4 \cdot 4\pi\, dr$$

for $Q \cdot \underbrace{\sqrt{\langle r^2 \rangle}}_{r_p} \ll 1$ we can make expansion in $Q \cdot r_p$

$$G_E(Q^2) = \int e^{i\vec{Q}\cdot\vec{r}}\, 4\pi \rho(r) r^2 dr \quad \text{(assuming spherical symmetry)}$$

$$= 4\pi \int \rho(r) \frac{\sin(Q\cdot r)}{Q\cdot r} r^2 dr$$

expanding the sin (or the exponential) we get (see Frauenfelder and Henley, e.g.)

$$G_E(Q^2) = 1 - \frac{1}{6} Q^2 \langle r^2 \rangle$$

$$\Rightarrow \quad \langle r^2 \rangle = -6 \cdot \frac{dG_E(Q^2)}{dQ^2}\Big|_{Q=0}$$

So the derivative $\frac{dG_E}{dQ^2}\Big|_{Q=0}$ determines the rms radius of the charge distribution

nucleon form factors, the latest news

EPJ Web of Conferences **81**, 01006 (2014)
DOI: 10.1051/epjconf/ 20148101006

EM Form Factors and OLYMPUS

Michael Kohl[1,2,a] for the OLYMPUS Collaboration

Q^2 dependence of proton form factors – about 2014 (Kohl)

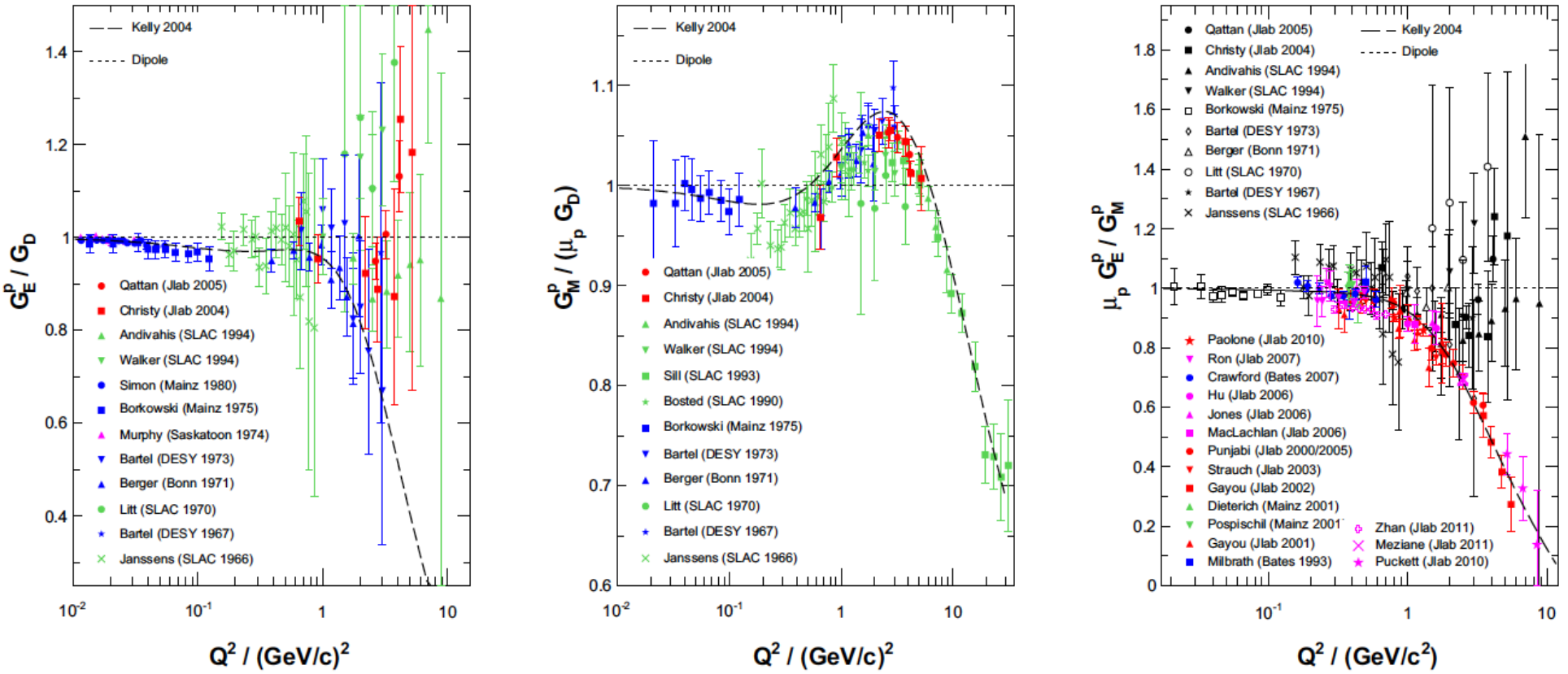

Left: Proton electric form factor G_E^p from Rosenbluth separation and forward-angle measurements [2, 3] normalized to the dipole form factor $G_D = (1 + Q^2/0.71)^{-2}$. Middle: Proton magnetic form factor G_M^p from Rosenbluth separation, backward-angle, and high-Q^2 cross section measurements [2, 4]. Right: Proton electric to magnetic form factor ratio from Rosenbluth-separated cross sections (black symbols) [2] and from double polarization experiments (colored symbols) [6, 7]. The Mainz Rosenbluth data [8, 9] are not shown.

[1] R. Hofstadter, Rev. Mod. Phys. **28**, 214 (1956).

[2] G_E^p and G_M^p from Rosenbluth separation: I.A. Qattan *et al.*, Phys. Rev. Lett. **94**, 142301 (2005); M.E. Christy *et al.*, Phys. Rev. C **70**, 015206 (2004); L. Andivahis *et al.*, Phys. Rev. D **50**, 5491 (1994); R.C. Walker *et al.*, Phys. Rev. D **49**, 5671 (1994); F. Borkowski *et al.*, Nucl. Phys. A **222**, 269 (1974); Nucl. Phys. B **93**, 461 (1975); W. Bartel *et al.*, Nucl. Phys. B **58**, 429 (1973); C. Berger *et al.*, Phys. Lett. B **35**, 87 (1971); J. Litt *et al.*, Phys. Lett. B **31**, 40 (1970); T. Janssens *et al.*, Phys. Rev. **142**, 922 (1966).

[3] G_E^p from forward-angle cross section: G.G. Simon *et al.*, Nucl. Phys. A **333**, 381 (1980); J.J. Murphy, Y.M. Shin, and D.M. Skopik, Phys. Rev. C **9**, 2125 (1974).

[4] G_M^p from large-angle or high-Q^2 cross section: A.F. Sill *et al.*, Phys. Rev. D **48**, 29 (1993); P.E. Bosted *et al.*, Phys. Rev. C **42**, 38 (1990).

[5] J.J. Kelly, Phys. Rev. C **70**, 068202 (2004).

[6] Ratio $\mu_p G_E^p/G_M^p$ from polarized target: C.B. Crawford *et al.*, Phys. Rev. Lett. **98**, 052301 (2007); M.K. Jones *et al.*, Phys. Rev. C **74**, 035201 (2006).

[7] Ratio $\mu_p G_E^p/G_M^p$ from recoil polarization, Jlab/Hall C at high Q^2: A.J.R. Puckett *et al.*, Phys. Rev. Lett. **104**, 242301 (2010); M. Meziane *et al.*, Phys. Rev. Lett. **106**, 132501 (2011); Jlab/Hall A at high Q^2: V. Punjabi *et al.*, Phys. Rev. C **71**, 055202 (2005); Erratum-ibid. Phys. Rev. C **71**, 069902(E) (2005) superseding M. Jones *et al.*, Phys. Rev. Lett. **84**, 1398 (2000); O. Gayou *et al.*, Phys. Rev. Lett. **88**, 092301 (2002); Jlab/Hall A at low Q^2: X. Zhan *et al.*, Phys. Lett. B **705**, 59 (2011); G. Ron *et al.*, Phys. Rev. Lett. **99**, 202002 (2007); B. Hu *et al.* Phys. Rev. C **73**, 064004 (2006); S. Strauch *et al.*, Phys. Rev. Lett. **91**, 052301 (2003); O. Gayou *et al.*, Phys. Rev. C **64**, 038202 (2001); G. MacLachlan *et al.*, Nucl. Phys. A **764**, 261 (2006); MAMI: T. Pospischil *et al.*, Eur. Phys. J. A **12**, 125 (2001); S. Dieterich *et al.*, Phys. Lett. B **500**, 47 (2001); MIT-Bates: B. Milbrath *et al.*, Phys. Rev. Lett. **80**, 452 (1998); Erratum-ibid. Phys. Rev. Lett. **82**, 2221(E) (1999).

[8] J.C. Bernauer *et al.*, Phys. Rev. Lett. **105**, 242001 (2010).

[9] J.C. Bernauer *et al.*, Phys. Rev. C **90**, 015206 (2014).

neutron form factors

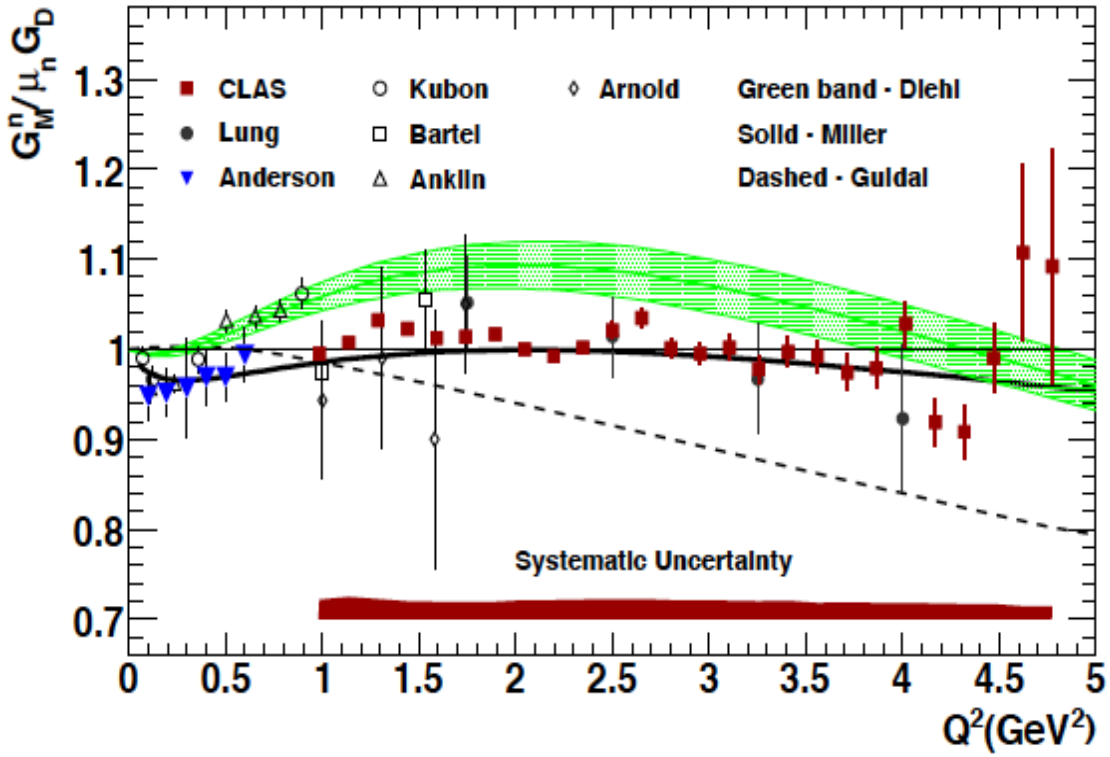

magnetic formfactor - close to dipole shape

CLAS coll., Phys.Rev.Lett. 102 (2009) 192001

neutron form factors

electric form factor - Mainz MAMI

Phys.Rev.Lett. 111 (2013) 13, 13250

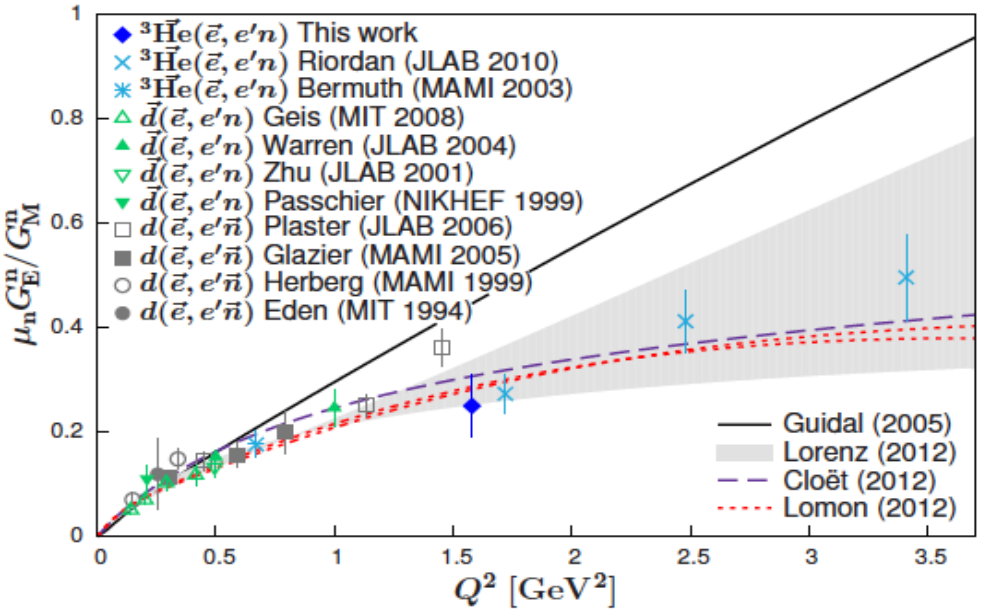

FIG. 3. (Color online) The result for $\mu_n G_E^n/G_M^n$ of this experiment along with results from other double polarization experiments [3–12]. The uncertainties shown are the statistical and the systematic errors added in quadrature. Also shown are the results of recent calculations based on general parton distributions [32] (solid line), dispersion analysis [33] (gray band), a quark-diquark model with a pion cloud [34] (dashed line) and the extended Lomon-Gari-Krümpelmann model of nucleon electromagnetic FF [35] (dotted lines, for two different parametrizations of resonance widths, timelike proton form factor data from *BABAR* included).

transverse density distribution of proton and neutron

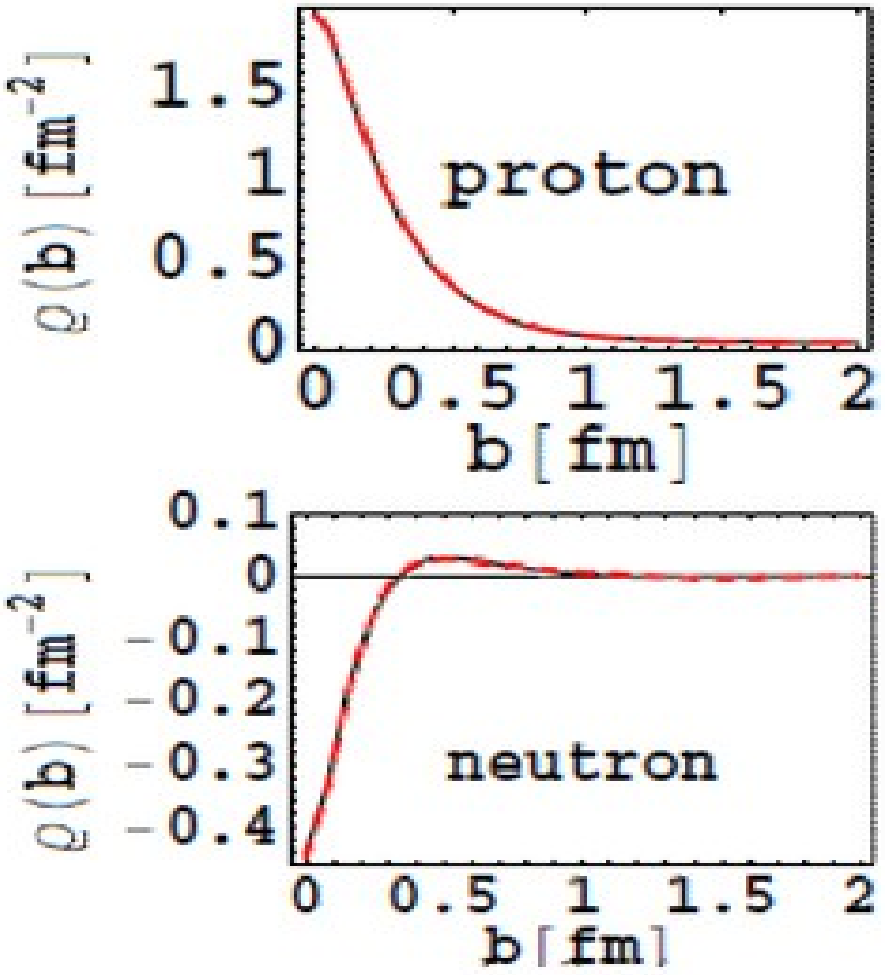

Miller G.A., Phys. Rev. Lett. 99, 112001 (2007)

the proton radius puzzle, about 2010, compiled by Richard Hill, arXiv:1702.01189

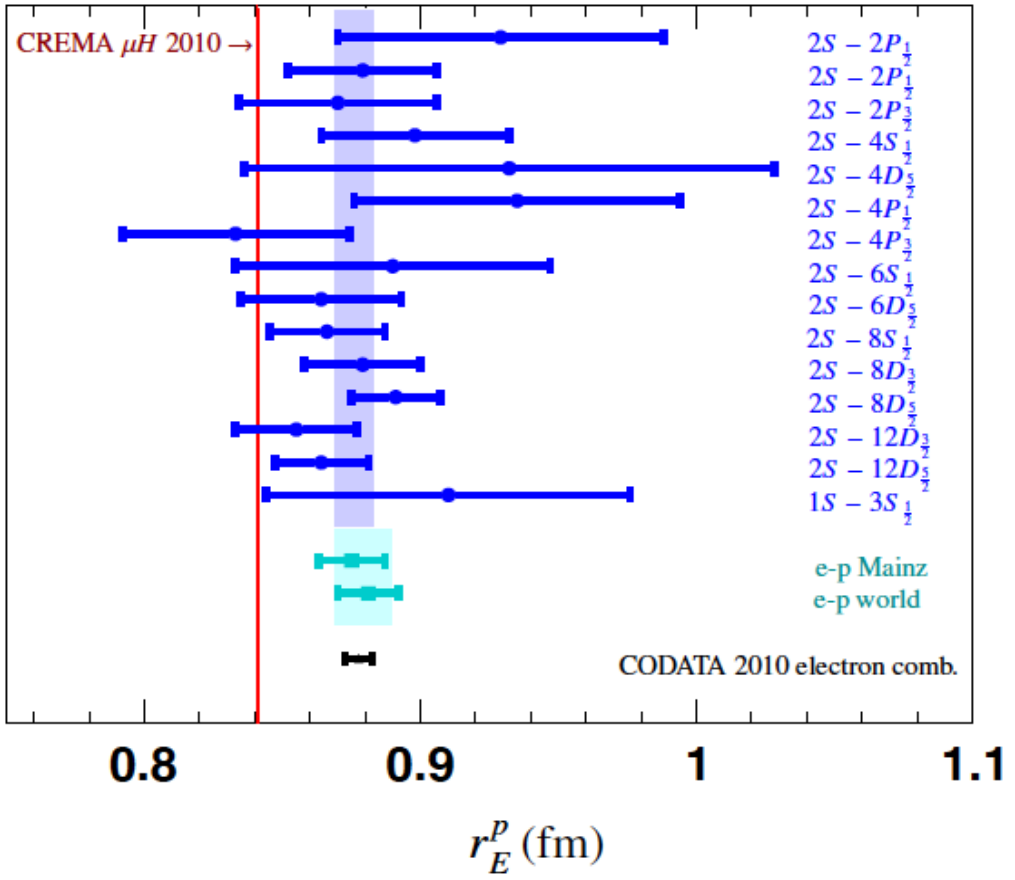

the red line is the result from μH measurements, the blue uncertainties come from H spectroscopy for various transitions, the turquoise result is from ep scattering, the black is the CODATA combination for all ep scattering data. The μH measurements are nearly 5.6 sigma below the CODATA evaluation.

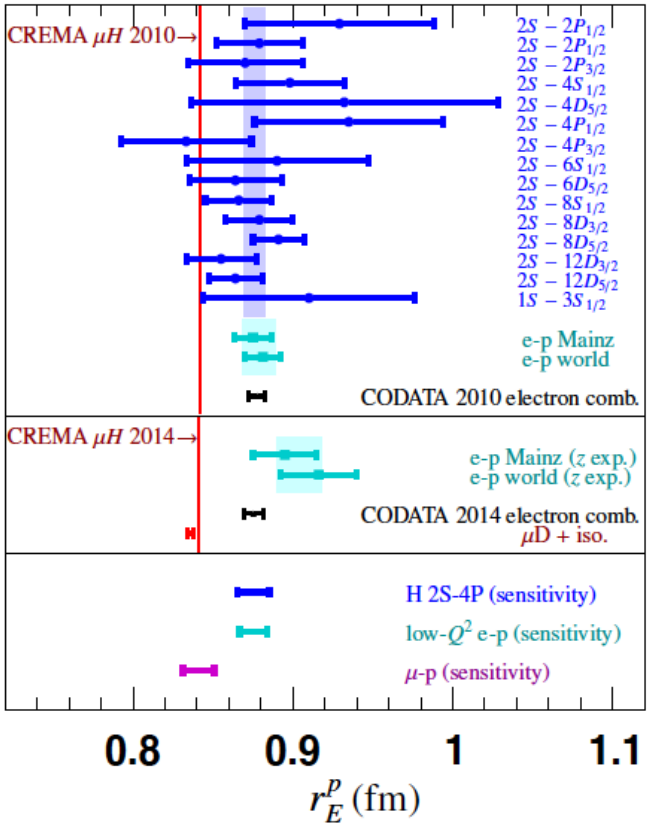

Status of the proton radius puzzle circa 2016, with prospects for new data. The upper pane is reproduced from Fig. 1. The middle pane shows updated results. The cyan points give updated fits to electron scattering data using z expansion (final two points in Fig. 4, from Ref. [15]. The black point represents the 2014 CODATA [1] combination of hydrogen and electron-proton scattering determinations. The red point is from the 2016 CREMA muonic deuterium Lamb shift measurement using the regular hydrogen-deuterium isotope shift [73]. The bottom pane shows expected sensitivities of anticipated results in: regular hydrogen [78] (blue); low-Q^2 electron-proton scattering [90] (cyan); and muon-proton scattering [92] (magenta). See text for details.

energy correction of H levels due to finite size of the proton,
see, e.g. Pohl, R., Nez, F., Udem, T., et al. 2016, arXiv:1607.03165

$$E_{n,\ell} \sim -\frac{R_\infty}{n^2} + \delta_{\ell 0}\frac{\left(r_E^p\right)^2}{n^3}$$

note: shift is only for s waves, other waves vanish at origin

why is sensitivity so enhanced in μH compared to eH?

$$\frac{|\psi_{\mu H}(0)|^2}{|\psi_{eH}(0)|^2} \sim \frac{m_\mu^3}{m_e^3} \sim (200)^3$$

because of large mass ratio $m_\mu/m_e \sim 200$, the radius sensitivity is much reduced, corresponding to a wave function much enhanced at the origin for μH

The idea of the Mainz experiment

in the scattering experiment, we know the incoming electron energy $E_0 = E_{beam}$, and the scattered electrons energy E' and angle θ'

then define: $Q^2_{in} = \frac{4E_0^2 \sin^2\frac{\theta'}{2}}{1 + \frac{2E_0}{M}\sin^2\frac{\theta'}{2}}$ $\quad Q^2_{out} = \frac{4E'^2 \sin^2\frac{\theta'}{2}}{1 - \frac{2E'}{M}\sin^2\frac{\theta'}{2}}$

the (small) terms in the denominator are 'recoil corrections' for cm $\leftrightarrow$ lab conversion

if 'Bethe-Heitler' photons and bremsstrahlung in the material of and around the target are neglected, then $Q_0^2 = 4E_0E'\sin^2\theta/2 = Q^2_{in} = Q^2_{out}$ and represents the actual value of Q^2 transferred to the proton.

In reality, the process is $H(e,e')pp$. In the initial state radiation (ISR) process (see fig.) the ISR photon removes energy from the incoming electron, to probe the proton at $Q^2 = Q^2_{out} < Q^2_0$. Because the ISR photons are soft, the photon cannot be measured and the process needs to be isolated by Monte Carlo simulation. This is the difficult but crucial part of the Mainz experiment. For details see: arXiv:1905.11182

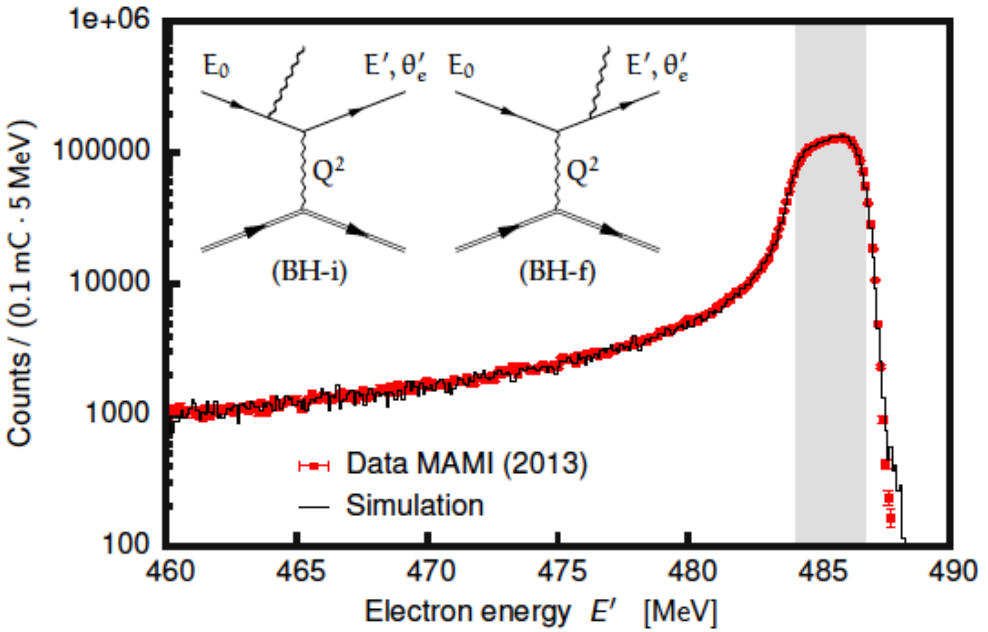

Figure 1: Measured and simulated elastic peak with the corresponding radiative tail for the first kinematic setting at 495 MeV. See [9] for details. The radiative tail is dominated by the two Bethe-Heitler diagrams (BH-i and BH-f), where electrons emit real photons before or after the interaction with the protons. The grey band marks the position and width of the elastic line inside the spectrometer acceptance.

The idea behind the JLAB experiment

eliminate as much as possible the material around the target with a windowless H gas cell

do not use magnetic spectrometer

measure instead the scattered electron with a combination of calorimetry and a high resolution GEM detector

For details see: Nature 575 (2019) 7781, 147

the PRAD experiment

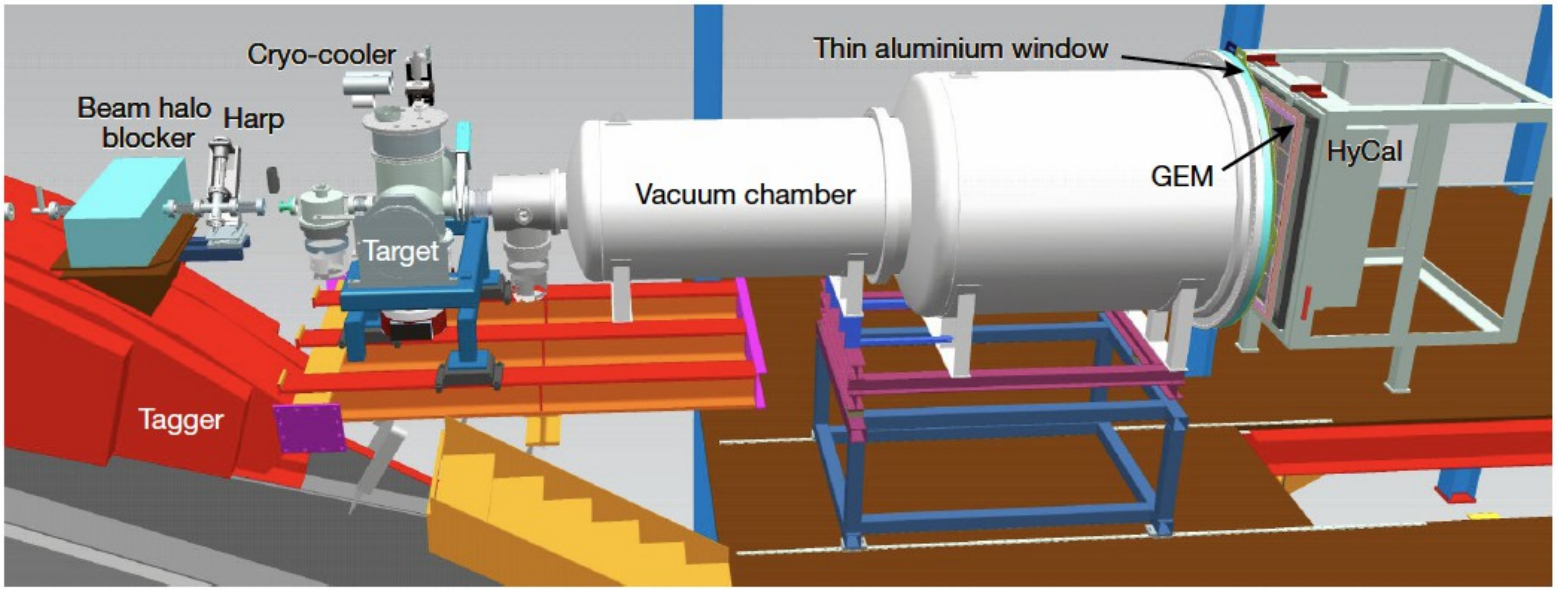

Fig. 1 | The PRad experimental setup. A schematic layout of the PRad experimental setup in Hall B at Jefferson Laboratory, with the electron beam incident from the left. The key beam-line elements are shown along with the windowless hydrogen gas target, the two-segment vacuum chamber and the two detector systems (see the Methods for a brief overview and the Supplementary Information for a description of the target and individual detectors).

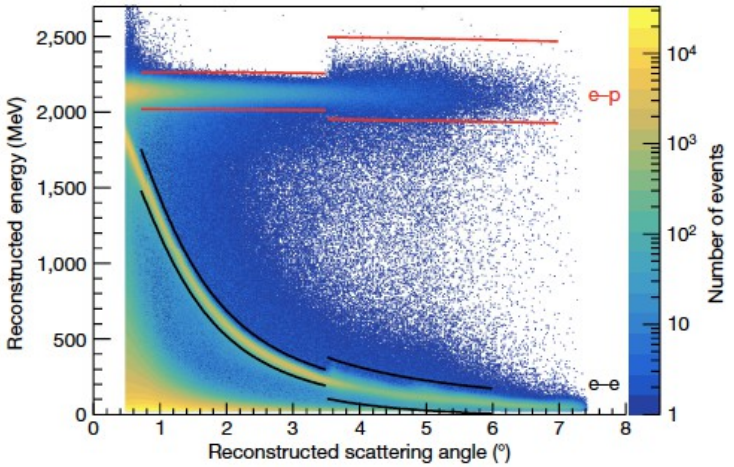

Fig. 2 | Event reconstruction. The reconstructed energy versus angle for e–p and e–e events for an electron beam energy of 2.2 GeV. The red and black lines indicate the event selections for e–p and e–e, respectively. The angles ≤3.5° are covered by the crystal $PbWO_4$ modules of HyCal and the larger angles by the Pb glass modules. The colour bar shows the number of events.

the PRAD experiment

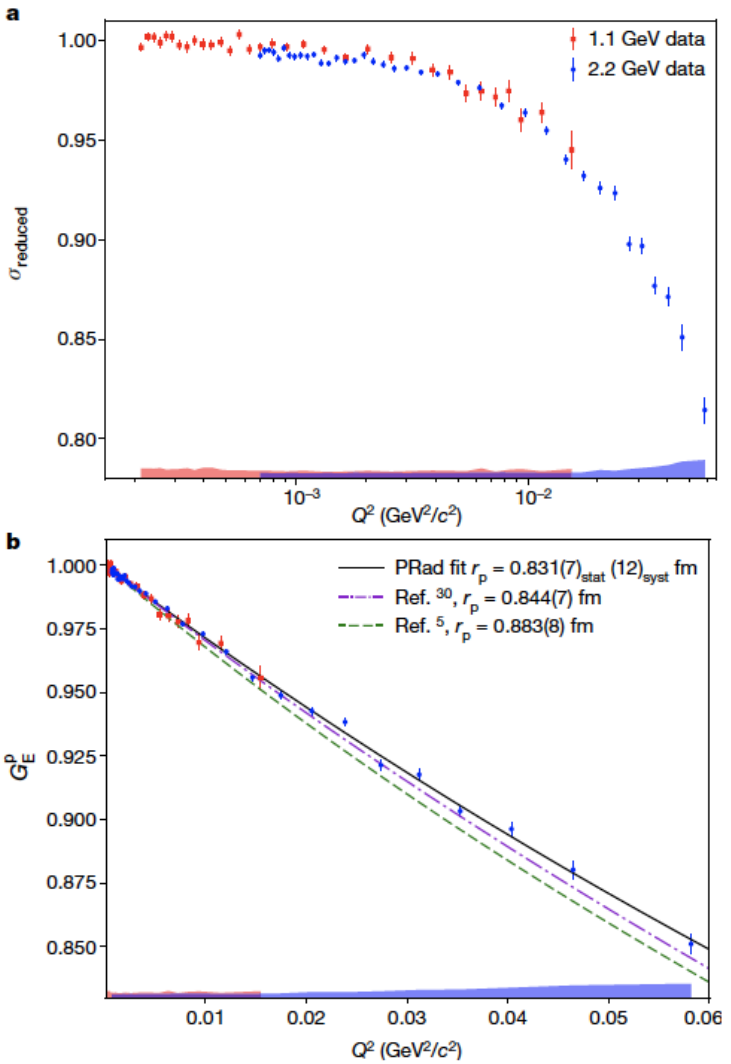

Fig. 3 | The measured cross-section and form factor. a, The reduced cross-section, $\sigma_{\text{reduced}} = \left(\frac{d\sigma}{d\Omega}\right)_{e\text{-}p} / \left[\left(\frac{d\sigma}{d\Omega}\right)_{\text{point-like}} ((4M_p^2E'/E)/(4M_p^2+Q^2))\right]$, (where E is the electron beam energy, E' is the energy of the scattered electron, M_p is the mass of the proton and Ω is the solid angle subtended by the scattered electron detector), for the PRad e–p data. Dividing out the kinematic factor inside the square brackets, σ_{reduced} is a linear combination of the electromagnetic form factors squared. The bands at the bottom of the plot are the size of the systematic uncertainties, for 1.1 GeV (red) and 2.2 GeV (blue). The error bars show statistical uncertainties. **b**, G_E^p as a function of Q^2. The data points are normalized by the parameter n in equation (1) for the 1.1-GeV and 2.2-GeV data, labelled as n_1 and n_2, respectively. The error bars show statistical uncertainties. The bands are the systematic uncertainties as in **a**. The solid black curve shows $G_E^p(Q^2)$ as a fit to the function given by equation (1). Also shown is the fit from a previous e–p experiment[5], giving $r_p = 0.883(8)$ fm (green dashed line) and another previous calculation[30] giving $r_p = 0.844(7)$ fm (purple dot-dashed line).

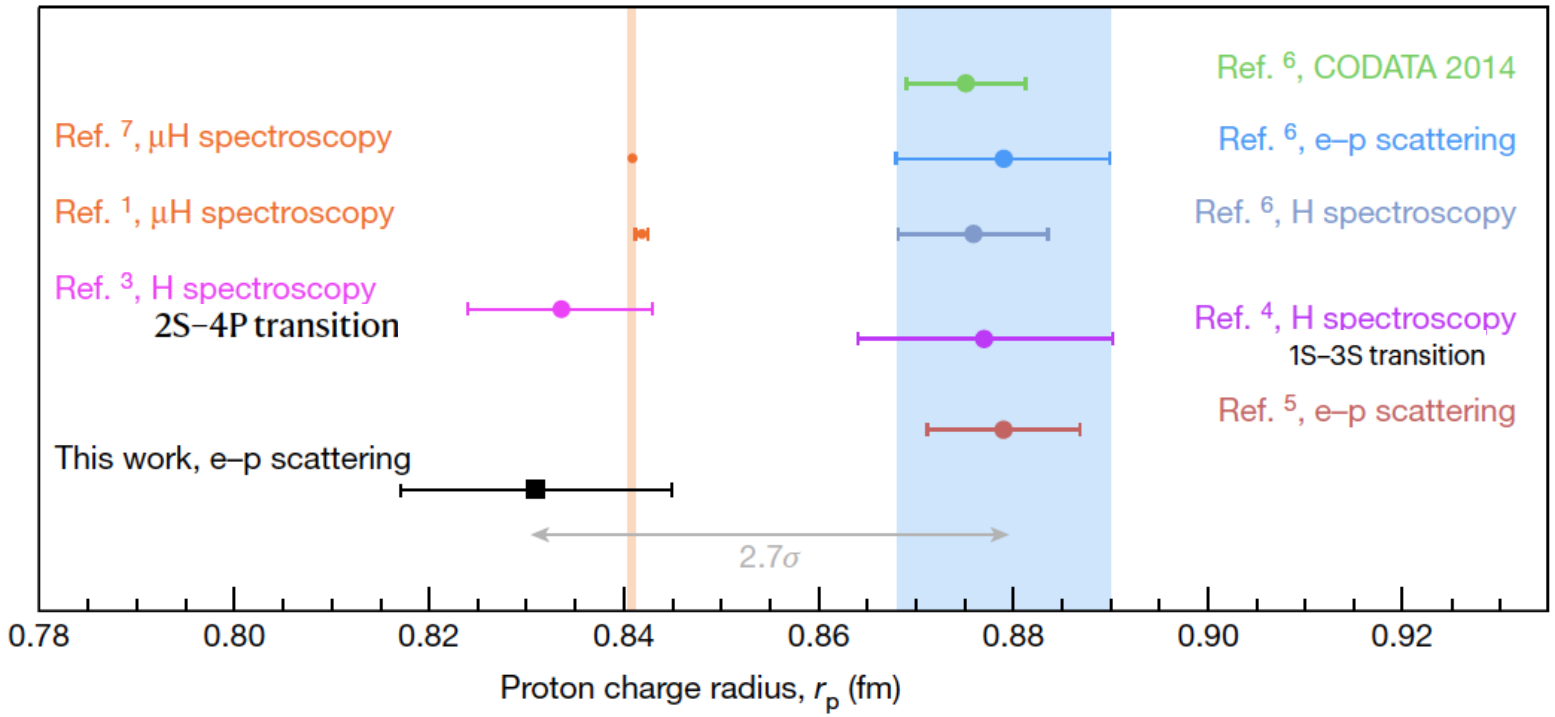

JLAB PRAD
Nature 571
(2019) no. 7781,147

situation in 2020

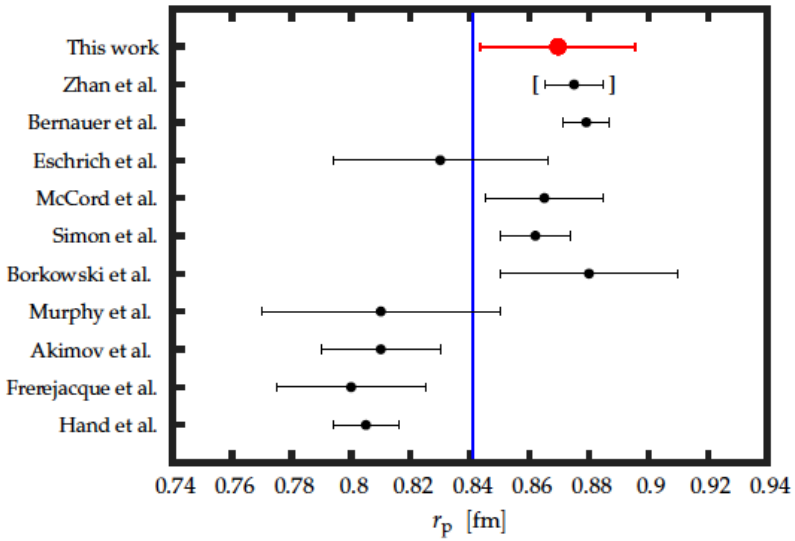

MAMI
arXiv:1905.11182

the two most recent measurements from electron scattering are consistent and consistent with the μH measurement but is the puzzle really solved? The discrepancy between the 2 most recent hydrogen spectroscopy results remains.

Refs. for the previous slide

1. Pohl, R. et al. The size of the proton. *Nature* **466**, 213–216 (2010).
2. Mohr, P. J., Taylor, B. N. & Newell, D. B. CODATA recommended values of the fundamental physical constants: 2006. *Rev. Mod. Phys.* **80**, 633–730 (2008).
3. Beyer, A. et al. The Rydberg constant and proton size from atomic hydrogen. *Science* **358**, 79–85 (2017).
4. Fleurbaey, H. New measurement of the 1S–3S transition frequency of hydrogen: contribution to the proton charge radius puzzle. *Phys. Rev. Lett.* **120**, 183001 (2018).
5. Bernauer, J. C. et al. High-precision determination of the electric and magnetic form factors of the proton. *Phys. Rev. Lett.* **105**, 242001 (2010).
6. Mohr, P. J., Newell, D. B. & Taylor, B. N. CODATA recommended values of the fundamental physical constants: 2014. *J. Phys. Chem. Ref. Data* **45**, 043102 (2016).
7. Antognini, A. et al. Proton structure from the measurement of 2S–2P transition frequencies of muonic hydrogen. *Science* **339**, 417–420 (2013).
8. Mohr, P. J., Newell, D. B. & Taylor, B. N. CODATA recommended values of the fundamental physical constants: 2018. http://physics.nist.gov/constants (2019).

most recent results based on:
Gao and Vanderhaeghen, Rev. Mod. Phys. 94 (2022) 1, 015002
2105.00571 [hep-ph]

the following figures are all taken from this paper

comparison of proton electric formfactor measurements over the last 60 years

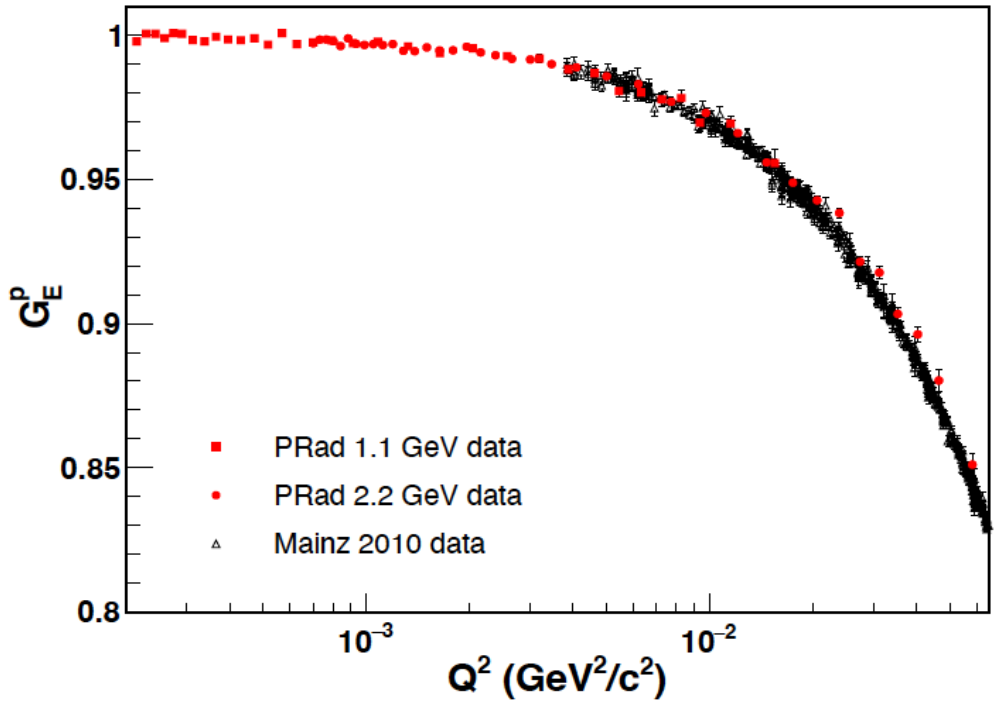

The proton electric form factor G_E^p from the PRad experiment together with those from the Mainz experiment (Bernauer *et al.*, 2010) in the overlap Q^2 region (figure credit: Weizhi Xiong).

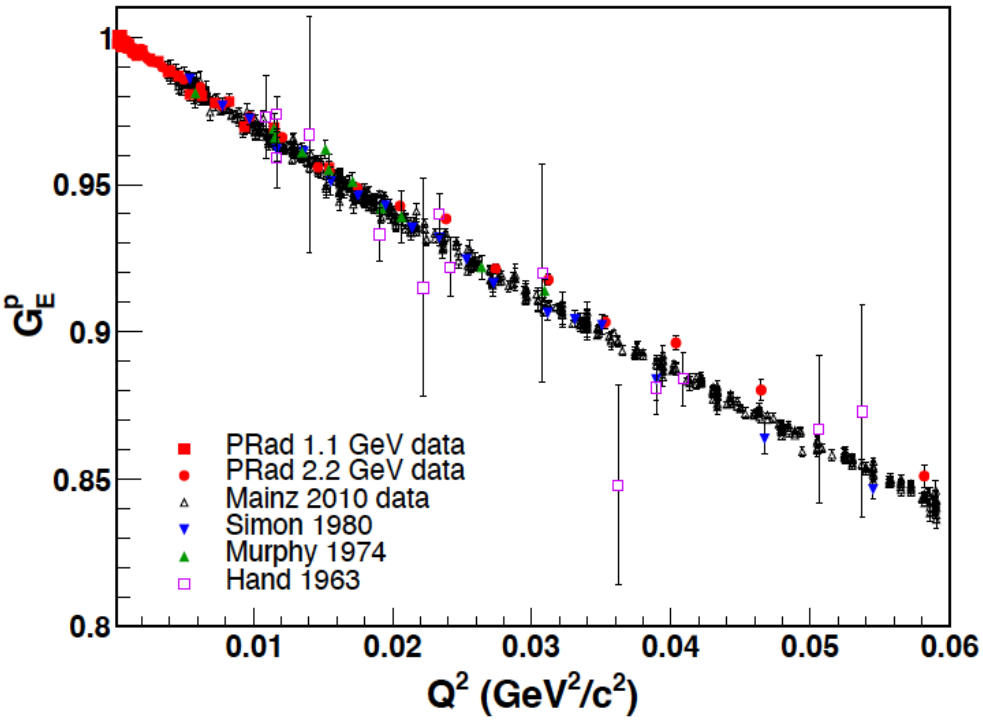

The proton electric form factor G_E^p from the PRad experiment together with those from (Bernauer *et al.*, 2010; Hand and Wilson, 1963; Murphy *et al.*, 1974b; Simon *et al.*, 1980) in the overlap Q^2 region, on linear scale (figure credit: Weizhi Xiong).

extraction of the proton charge radius from the measured electric formfactor

the PRad collaboration bases its radius extraction on the method developed in
X. Yan et al, Phys. Rev. C 98 (2018) 2, 025204
1803.01629 [nucl-ex]

main idea: create a general framework for studying various form-factor functions along with various fitting functions. The input form factors are used to generate pseudo-data with fluctuations mimicking the binning and random uncertainty of a set of real data. All combinations of input functions and fit functions can then be tested repeatedly against regenerated pseudo-data. Since the input radius is known, this allows us to find fitting functions that are robust for proton radius extractions in an objective fashion.

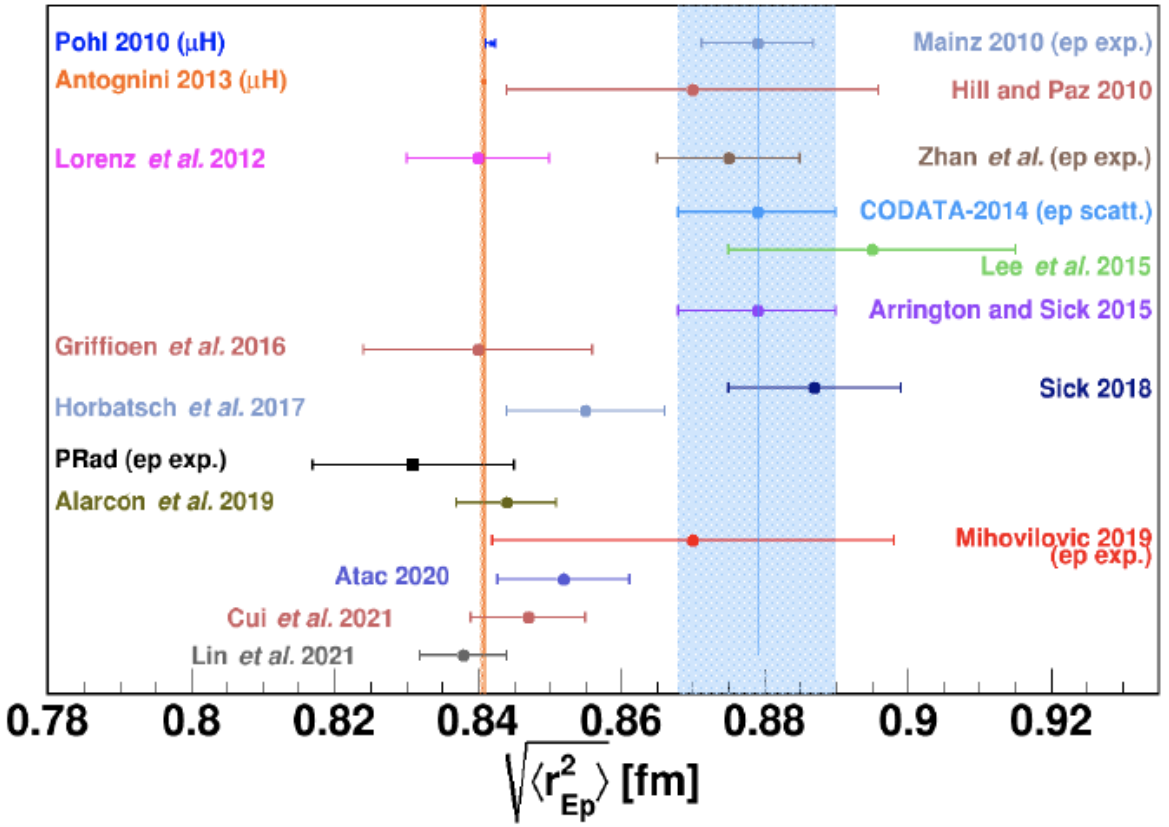

The proton charge radius values determined from electron scattering experiments since 2010 together with the results from the various analyses of electron-proton scattering data (see text) (figure credit: Jingyi Zhou).

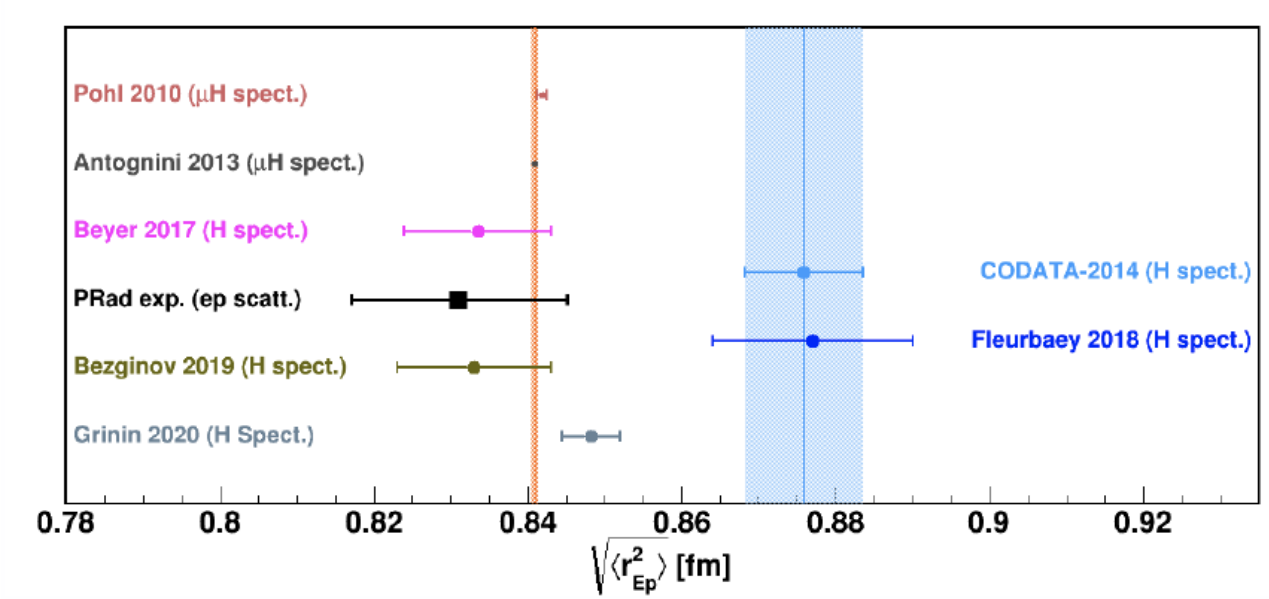

The latest proton charge radius results from ordinary hydrogen spectroscopic measurements together with muonic hydrogen results and the CODATA-2014 recommended value based on ordinary hydrogen spectroscopy and the most recent result from electron scattering (figure credit: Jingyi Zhou).

the Prad-II experiment:
improving the precision by about a factor of 4

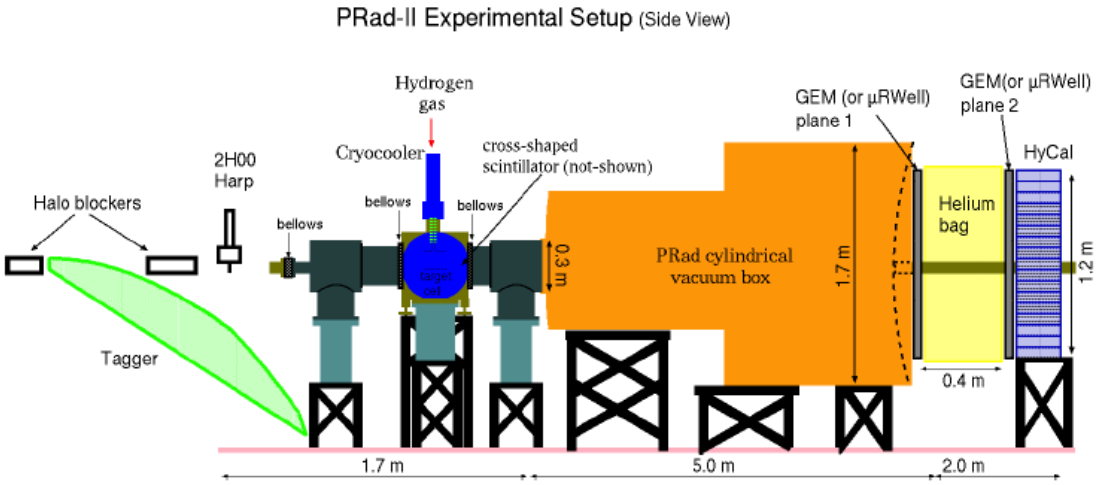

Schematic of the setup for the proposed PRad-II experiment. The incident electron beam is from left to right (figure credit: Dipangkar Dutta).

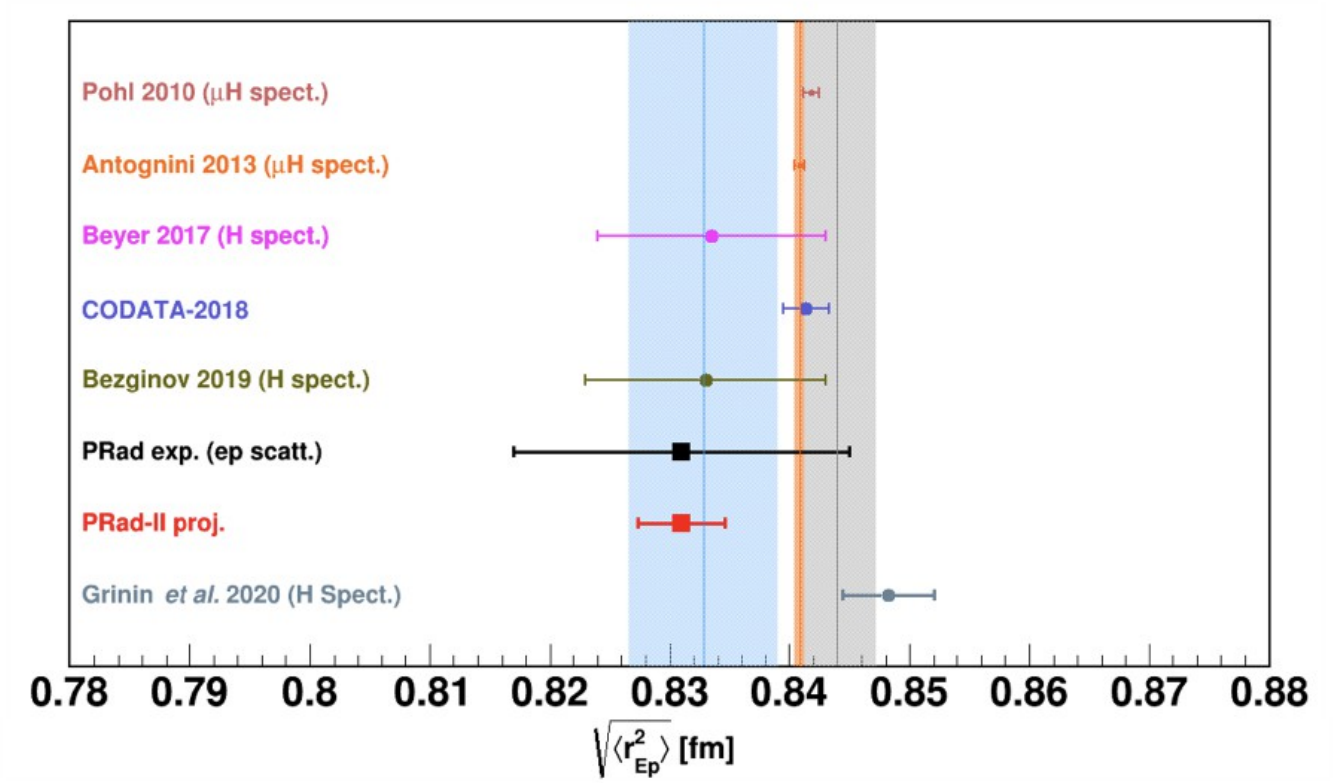

The PRad-II projection for $\langle r^2_{Ep} \rangle^{1/2}$ with all proposed upgrades and improvements shown with a few selected results from other experiments and CODATA-2018 recommendations (see text) (figure credit: Jingyi Zhou).